Available online at www.sciencedirect.com
SCIENCE DIRECT®
International Journal of Solids and Structures 42 (2005) 2381–2398
INTERNATIONAL JOURNAL OF SOLIDS and STRUCTURES
www.elsevier.com/locate/ijsolstr

Dynamics of an axially moving viscoelastic beam subject to axial tension

Usik Lee [a,*], Hyungmi Oh [a]

[a] *Department of Mechanical Engineering, Inha University, 253 Yonghyun-Dong, Nam-Ku, Incheon 402-751, Republic of Korea*

Received 15 December 2003; received in revised form 19 September 2004
Available online 2 November 2004

Abstract

In this paper, a spectral element model is derived for the dynamics and stability analyses of the axially moving viscoelastic beams subject to axial tension. The viscoelastic material is represented in a general form by using the one-dimensional constitutive equation of hereditary integral type. The high accuracy of the present spectral element model is verified first by comparing the eigenvalues obtained by the present spectral element model with those obtained by using the conventional finite element model as well as with the exact analytical solutions. The effects of viscoelasticity and moving speed on the dynamics and stability of moving beams are numerically investigated.

Keywords: Moving beam; Viscoelastic beam; Spectral element matrix; Spectral element method; Dynamic and stability; Critical moving speed; Divergence; Flutter

1. Introduction

The moving belt used in power transmissions is an example of axially moving one-dimensional structures. Above a certain critical moving speed, such axially moving structures may experience severe vibrations and dynamical instabilities to cause structural failures. To ensure that such structural systems are under stable working conditions, the dynamic responses and stability of such systems have been studied extensively. In most existing previous works, the axially moving one-dimensional structures were assumed

* Corresponding author. Tel.: +82 32 860 7318; fax: +82 32 866 1434.
E-mail address: ulee@inha.ac.kr (U. Lee).

0020-7683/$ - see front matter © 2004 Elsevier Ltd. All rights reserved.
doi:10.1016/j.ijsolstr.2004.09.026

to be elastic and represented by string models or beam models. An extensive literature overview on this subject can be found from Wickert and Mote (1988).

With the advancement of material technologies, new materials such as plastics, metallic or ceramic reinforced composite materials and polymeric materials are now widely used for moving belts (e.g., Fung et al., 1997; Zhang and Zu, 1998, 1999; Hou and Zu, 2002; Marynowski and Kapitaniak, 2002). Such materials do not obey Hook's law, but exert inherently viscoelastic behavior which can be modeled by integral or differential type of constitutive equations (Flügge, 1975; Christensen, 1982; Haddad, 1995). However, to the authors' surprises, the literature that is specially related to a viscoelastic moving structures is found to be very limited. Fung et al. (1997) seems to be the first to discuss the transverse vibration of a viscoelastic moving belt of which material was modeled by a standard linear solid model of hereditary integral type. They used a Galerkin's method and a finite difference numerical integration procedure to obtain the transient responses. Later on, Fung et al. (1998) extended their previous work to investigate the effect of material damping on the nonlinear free vibration of moving belts, while Zhang and Zu (1998, 1999) considered the nonlinear free and forced vibrations and parametrically excited oscillations by adopting a Kelvin model of differential type for the viscoelastic material of moving belt. Hou and Zu (2002) used a standard linear solid model of differential type to investigate the nonlinear free oscillations of moving viscoelastic belts. In the aforementioned references, the moving viscoelastic belts were all represented by string models. The beam model was used by Marynowski and Kapitaniak (2002) to investigate the stability and oscillations of an axially moving viscoelastic web by using the Runge–Kutta method. They used the differential type of constitutive equations for the viscoelastic material of web.

In the literature, various solution methods have been presented for the vibration analysis of linear viscoelastic structures; for instance, Galerkin's method (e.g., Fung et al., 1997), Runge–Kutta method (e.g., Marynowski and Kapitaniak, 2002), Laplace transform method (e.g., Flügge, 1975), the correspondence and superposition principles (e.g., Findley et al., 1976), Fourier transform method (e.g., Christensen, 1982), finite element method (e.g. White, 1986), hybrid Laplace transform/finite element method (e.g., Chen, 1995), and so forth.

The spectral element method (SEM) is an exact solution method for the dynamic analysis of structures (Doyle, 1997; Lee et al., 2000; Lee, 2004). In SEM, the FFT-techniques based on spectral element matrix (often called 'exact dynamic stiffness matrix') are used to obtain dynamic responses in the frequency- and time-domains. The spectral element matrix is formulated in the frequency-domain by using the frequency-dependent dynamic shape functions satisfying governing structural dynamic equations. Thus, it allows one to use only one finite element for a uniform structure, regardless of its length. The conventional finite element assembly procedure can be equally used in SEM to formulate the system equation of complicated structures. In SEM, the dynamic responses in frequency- and time-domains are computed very efficiently by using the forward-FFT (simply, FFT) and inverse-FFT (simply, IFFT) algorithms. The use of FFT-techniques may improve the solution accuracy considerably, while reducing the computational costs. Because the SEM is a frequency-domain method, it seems to be best fit for viscoelastic structures of which material properties are most often extracted indirectly from the experimental forced vibration responses given in the form of receptance frequency response functions (FRF) (e.g., Dalenbring, 2003). Although the spectral element matrix for the axially moving zelastic string was recently derived by Le-Ngoc and McCallion (1999) to obtain exact eigenvalues, the spectral element matrix for the axially moving viscoelastic beam has not been published in the literature.

Thus, the purposes of this paper are to develop a spectral element model for the axially moving viscoelastic beams subject to axial tension, and to investigate the effects of viscoelasticity and moving speed on the vibration and stability of an example moving viscoelastic beam.

2. Equation of motion

2.1. Constitutive equation

The three-dimensional constitutive equation for an integral type anisotropic linearly viscoelastic material is given by (Christensen, 1982)

$$\sigma_{ij}(t) = \int_{-\infty}^{t} r_{ijkl}(t-\tau)\dot{\varepsilon}_{kl}(\tau)\,\mathrm{d}\tau = r_{ijkl}(t) * \mathrm{d}\varepsilon_{kl}(t), \tag{1}$$

where $\sigma_{ij}(t)$ is the tensor of stress history, $\varepsilon_{ij}(t)$ is the tensor of strain history, $r_{ijkl}(t)$ is the fourth order tensor of relaxation function, and $(*)$ denotes the Stieltjes convolution between $r_{ijkl}(t)$ and $\mathrm{d}\varepsilon_{ij}(t)$.The dot $(\cdot)$ denotes the derivative with respective to time t. For the one dimensional isotropic linearly viscoelastic material, (1) can be reduced to

$$\sigma(t) = \int_{-\infty}^{t} r(t-\tau)\dot{\varepsilon}(\tau)\,\mathrm{d}\tau = r(t) * \mathrm{d}\varepsilon(t). \tag{2}$$

In the frequency-domain, (2) can be expressed as

$$\sigma(\omega) = \mathrm{i}\omega R(\omega)\varepsilon(\omega), \tag{3}$$

where $\mathrm{i} = \sqrt{-1}$ is the imaginary unit, ω is the circular frequency, and $\sigma(\omega)$, $\varepsilon(\omega)$ and $R(\omega)$ are the Fourier transforms of the stress history $\sigma(t)$, strain history $\varepsilon(t)$, and relaxation function $R(t)$, respectively.

2.2. Equation of motion

Consider a uniform straight viscoelastic beam of length L, which travels at constant transport speed c under an applied axial tension P. The equation of motion and relevant boundary conditions can be derived from the extended Hamilton's principle (Abolghasemi and Jalali, 2003):

$$\int_{t_1}^{t_2} (\delta K - \delta V + \delta W)\,\mathrm{d}t = 0. \tag{4}$$

The kinetic energy K and the potential energy V are given by

$$\begin{aligned} K &= \frac{1}{2}\int_0^L \rho A\{c^2 + (\dot{w} + cw')^2\}\,\mathrm{d}x, \\ V &= \frac{1}{2}\int_0^L (Mw'' + Pw'^2)\,\mathrm{d}x, \end{aligned} \tag{5}$$

where $w(x,t)$ is the transverse deflection, ρA is the mass per length, and M is the resultant bending moment of beam. In (5), the prime $(')$ denotes the derivative with respective to spatial coordinate x. The virtual work δW is given by

$$\delta W = \int_0^L f(x,t)\,\delta x + M_1\,\delta\theta_1 + M_2\,\delta\theta_2 + Q_1\,\delta w_1 + Q_2\,\delta w_2, \tag{6}$$

where $f(x,t)$ is the external force, and M_1, Q_1 and θ_1 are the bending moment, the transverse shear force, and the slope specified at $x = 0$, while M_2, Q_2 and θ_2 are those specified at $x = L$. The slopes θ_1 and θ_2 are related to the transverse deflection as

$$\theta_1(t) = w'(0,t), \qquad \theta_2(t) = w'(L,t). \tag{7}$$

Introducing (5) and (6) into the extended Hamilton's principle (4), and applying the integral by parts yields

$$\int_{t_1}^{t_2}\int_0^L \left[-M'' - \rho A(c^2 w'' + 2c\dot{w}' + \ddot{w}) + Pw'' + f(x,t)\right]\delta w\,\mathrm{d}x\,\mathrm{d}t + \int_{t_1}^{t_2}\left\{Q(x,t)\,\delta w|_0^L + Q_1\,\delta w_1 + Q_2\,\delta w_2\right\}\mathrm{d}t + \int_{t_1}^{t_2}\left\{-M(x,t)\,\delta\theta|_0^L + M_1\,\delta\theta_1 + M_2\,\delta\theta_2\right\}\mathrm{d}t = 0, \tag{8}$$

where $M(x,t)$ and $Q(x,t)$ are the resultant bending moment and transverse shear force, respectively, defined by

$$M(x,t) = \int_A -\sigma z\,\mathrm{d}A, \qquad Q(x,t) = M' + \rho A c(\dot{w} + cw') + Pw'. \tag{9}$$

From (8), the equation of motion for the moving viscoelastic beam can be obtained as

$$I\{R(t) * \dot{w}''''\} + \rho A(c^2 w'' + 2c\dot{w}' + \ddot{w}) - Pw'' = f(x,t) \tag{10}$$

with the relevant boundary conditions as

$$\begin{aligned} &w(0,t) = w_1 \quad \text{or} \quad Q(0,t) = Q_1,\\ &\theta(0,t) = \theta_1 \quad \text{or} \quad M(0,t) = -M_1,\\ &w(L,t) = w_2 \quad \text{or} \quad Q(L,t) = -Q_2,\\ &\theta(L,t) = \theta_2 \quad \text{or} \quad M(L,t) = M_2. \end{aligned} \tag{11}$$

Substituting (2) into (9) gives the relations:

$$M(x,t) = I(R * \dot{w}''), \qquad Q(x,t) = I(R * \dot{w}''') + \rho A c(\dot{w} + cw') - Pw'. \tag{12}$$

3. Spectral element formulation

The spectral element formulation begins with the governing equation of motion without external force. The general solution is then represented in the discrete Fourier transform (DFT) form as

$$w(x,t) = \sum_{n=0}^{N-1} W_n(x)\mathrm{e}^{\mathrm{i}\omega_n t}, \tag{13}$$

where $W_n(x)$ is the spectral components (or Fourier coefficients) corresponding to discrete frequencies $\omega_n = 2\pi n/T$ $(n = 0,1,2,\ldots,N-1)$, where N is the number of spectral components to be taken into account in the analysis, and T is the time window related to N as

$$N = 2f_{\mathrm{NYQ}}T, \tag{14}$$

where f_{NYQ} is the highest frequency called *Nyquist* frequency. The spectral components are arranged to satisfy $W_{N-n} = W_n^*$, where W_n^* is complex conjugate of W_n by the theory of DFT. The accuracy of time responses may depend on how many spectral components are taken into account in the analysis. The summation and subscripts used in (13) are so obvious that they will be omitted in the following equations for brevity.

By substituting (13) into (10), with $f(x,t) = 0$, one can obtain

$$\mathrm{i}\omega R(\omega) I W'''' - (P - \rho A c^2)W'' + 2\mathrm{i}\omega\rho A c W' - \rho A\omega^2 W = 0. \tag{15}$$

The general solution of (15), i.e., the nth specific spectral component, is assumed in the form as

$$W(x) = Ce^{ikx}, \tag{16}$$

where k is the wavenumber. Substituting (16) into (15) yields a dispersion relation:

$$i\omega R(\omega)Ik^4 + (P - \rho Ac^2)k^2 - 2\omega\rho Ack - \rho A\omega^2 = 0. \tag{17}$$

From (17), four roots k_r ($r = 1,2,3,4$) can be obtained. Then the general solution of (15) can be rewritten as

$$W(x) = \sum_{r=1}^{4} C_r e^{ik_r x}. \tag{18}$$

Now, consider a finite beam element of length l as shown in Fig. 1. The spectral nodal degrees of freedom (DOFs), the spectral nodal shear forces and the spectral nodal bending moments are listed in Fig. 1. The spectral nodal DOFs are defined by

$$\begin{aligned} W_1 &= W(0), \qquad \Theta_1 = W'(0), \\ W_2 &= W(l), \qquad \Theta_2 = W'(l). \end{aligned} \tag{19}$$

Substituting (18) into (19) gives a relation between the nodal DOFs vector $\boldsymbol{d}$ and the constants vector $\boldsymbol{C}$ as

$$\boldsymbol{d} = \boldsymbol{Y}(\omega)\boldsymbol{C}, \tag{20}$$

where

$$\begin{aligned} &\boldsymbol{d} = \{\, W_1 \quad \Theta_1 \quad W_2 \quad \Theta_2 \,\}^{\mathrm{T}}, \qquad \boldsymbol{C} = \{\, C_1 \quad C_2 \quad C_3 \quad C_4 \,\}^{\mathrm{T}}, \\ &\boldsymbol{Y}(\omega) = \begin{bmatrix} 1 & 1 & 1 & 1 \\ \varepsilon_1 & \varepsilon_2 & \varepsilon_3 & \varepsilon_4 \\ e_1 & e_2 & e_3 & e_4 \\ e_1\varepsilon_1 & e_2\varepsilon_2 & e_3\varepsilon_3 & e_4\varepsilon_4 \end{bmatrix} \end{aligned} \tag{21}$$

with the definitions of

$$\varepsilon_r = ik_r, \quad e_r = e^{ik_r l} \qquad (r = 1,2,3,4). \tag{22}$$

Assume that the shear force $Q(x,t)$ and bending moment $M(x,t)$ can be represented in the DFT forms as

$$Q(x,t) = \sum_{n=0}^{N-1} Q_n(x)e^{i\omega_n t}, \qquad M(x,t) = \sum_{n=0}^{N-1} M_n(x)e^{i\omega_n t}. \tag{23}$$

Applying (13) into (12) and using (23) gives the spectral components of $Q(x,t)$ and $M(x,t)$ as follows:

$$M(x) = i\omega R(\omega)W'', \qquad Q(x) = i\omega R(\omega)W''' + (\rho Ac^2 - P)W' + i\omega\rho AcW, \tag{24}$$

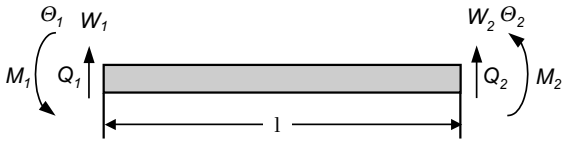

Fig. 1. Sign convention for the moving finite viscoelastic beam element.

where the subscript n is omitted for brevity. The nodal shear forces and nodal bending moments specified on the finite beam element shown in Fig. 1 are defined by

$$Q_1 = Q(0), \qquad M_1 = -M(0), \qquad Q_2 = -Q(l), \qquad M_2 = M(l) \tag{25}$$

Substituting (18) into (24) and applying the results into (25) yields a relation between the nodal forces vector $\boldsymbol{f}$ and the constants vector $\boldsymbol{C}$ as

$$\boldsymbol{f} = \boldsymbol{X}(\omega)\boldsymbol{C}, \tag{26}$$

where

$$f = \{\, Q_1 \quad M_1 \quad Q_2 \quad M_2 \,\}^{\mathrm{T}}, \qquad \boldsymbol{X}(\omega) = \begin{bmatrix} -g_1 & -g_2 & -g_3 & -g_4 \\ -h_1 & -h_2 & -h_3 & -h_4 \\ e_1 g_1 & e_2 g_2 & e_3 g_3 & e_4 g_4 \\ e_1 h_1 & e_2 h_2 & e_3 h_3 & e_4 h_4 \end{bmatrix} \tag{27}$$

with

$$g_r = -\mathrm{i}\left[\mathrm{i}\omega R(\omega) k_r^3 + (\rho A c^2 - P) k_r + \omega \rho A c\right], \qquad h_r = -\mathrm{i}\omega R(\omega) k_r^2. \tag{28}$$

The constants vector $\boldsymbol{C}$ can be readily eliminated from (20) and (26) to obtain the relation between the nodal forces vector and the nodal DOFs vector as follows:

$$\boldsymbol{f} = \boldsymbol{S}(\omega)\boldsymbol{d}, \tag{29}$$

where $\boldsymbol{S}(\omega)$ is the frequency-dependent spectral element matrix defined by

$$\boldsymbol{S}(\omega) = \boldsymbol{X}(\omega)\boldsymbol{Y}(\omega)^{-1}. \tag{30}$$

The spectral element matrices can be assembled in a completely analogous way to that used in the conventional FEM. Finally applying the boundary conditions may provide a global system equation in the form:

$$\boldsymbol{S}_g(\omega)\boldsymbol{d}_g = \boldsymbol{f}_g, \tag{31}$$

where $\boldsymbol{S}_g(\omega)$ is the global spectral matrix, $\boldsymbol{d}_g$ is the global spectral nodal DOFs vector, and $\boldsymbol{f}_g$ is the global spectral nodal forces vector.

The natural frequencies ω_{NAT} can be obtained from the condition that the determinant of global spectral matrix $\boldsymbol{S}_g(\omega)$ becomes zero as

$$\det \boldsymbol{S}_g(\omega_{\mathrm{NAT}}) = 0. \tag{32}$$

To compute the roots of (32), one may plot $\det \boldsymbol{S}_g(\omega)$ with respect to the frequency ω and/or use a proper root-finding algorithm. Not to miss any roots bellow a certain specified frequency during the root search process, the Wittrick–Williams algorithm (Wittrick and Williams, 1971) can be applied.

To obtain the dynamic responses in time-domain, first compute $\boldsymbol{f}_g$ from the external forces transformed into the frequency-domain by using the forward-FFT algorithm. Next solve (31) for $\boldsymbol{d}_g$ and apply the results into (20) to compute the spectral components of response from (18). Finally, based on the DFT theory of (13), the inverse-FFT algorithm is used to obtain the vibration response in the time-domain. One may remember that, because there have not been made any restriction on $R(\omega)$, the Fourier transform of relaxation function of a viscoelastic material, the spectral element matrix of (30) is general and can be applied to any linearly viscoelastic moving beams subjected to axial tension.

4. Numerical results and discussion

Numerical studies have been conducted to evaluate the present spectral element model as well as to investigate the effects of viscoelastcity and moving speed on the dynamics and stabilities of moving viscoelastic beams.

For the numerical studies, two beam models shown in Fig. 2 are considered: one-span beam (Fig. 2a) and two-span beam (Fig. 2b). The one-span beam is simply supported at both ends and the two-span beam is constructed by connecting two equal one-span beams so that its total length is twice the length of the original one- span beam. The mid-point and two ends of the two-span beam are all simply supported. Each span of beam has the length $L = 1\,\mathrm{m}$, width $b = 0.2\,\mathrm{m}$, thickness $h = 0.0015\,\mathrm{m}$, and mass density $\rho = 7800\,\mathrm{kg/m^3}$. The viscoelasticity of the beam material is represented by the Kelvin–Voigt model (see Fig. 3), which can be represented by (Flügge, 1975)

$$\sigma(t) = E\varepsilon(t) + \eta\dot{\varepsilon}(t). \tag{33}$$

Thus, the Fourier transform of the relaxation function of viscoelastic material can be obtained from (33) as by (Flügge, 1975):

$$\mathrm{i}\omega R(\omega) = E + \mathrm{i}\omega\eta. \tag{34}$$

For numerical computations, Young's modulus $E = 2 \times 10^{11}\,\mathrm{N/m^2}$ is used with varying the magnitude of viscoelasticity η.

4.1. Accuracy of spectral element model

The high accuracy of the present spectral element model is verified first by comparing the eigenvalues obtained by using the present SEM with those by the conventional FEM as well as with the exact analytical

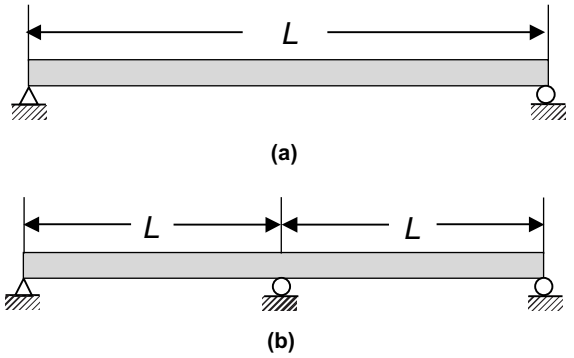

Fig. 2. Two stationary beams with simply supported boundary conditions. (a) One-span beam and (b) two-spans beam.

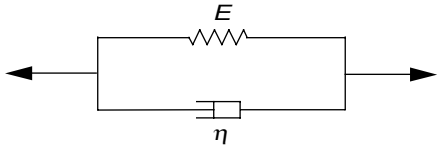

Fig. 3. Kelvin–Voigt model of the viscoelastic beam material.

results from (Karnovsky and Lebed, 2001). For this end, we assume that two example beams shown in Fig. 2 are stationary (i.e., $c = 0\,\mathrm{m/s}$), but not subject to the axial tension (i.e., $P = 0$ N). The finite element model used for the FEM results can be represented by

$$\boldsymbol{M}\ddot{\boldsymbol{d}} + (\boldsymbol{C}_{\mathrm{G}} + \boldsymbol{C}_{\mathrm{V}})\dot{\boldsymbol{d}} + \boldsymbol{K}\boldsymbol{d} = \boldsymbol{f} \tag{35}$$

where $\boldsymbol{d}$ is the nodal displacement DOFs vector defined by (20), $\boldsymbol{f}$ is the nodal forces vector, $\boldsymbol{M}$ is the mass matrix, $\boldsymbol{C}_{\mathrm{G}}$ is the skew-symmetric gyroscopic matrix, $\boldsymbol{C}_{\mathrm{V}}$ is the viscoelastic damping matrix, and $\boldsymbol{K}$ is the stiffness matrix. To formulate the finite element model given by (35), the displacement fields within a finite element of length l are assumed in the form (Petyt, 1990)

$$w(x,t) = \boldsymbol{N}(x)\boldsymbol{d}(t), \tag{36}$$

where $\boldsymbol{N}(x)$ is the shape function matrix given by

$$\boldsymbol{N}(x) = \left[1 - 3\xi^2 + 2\xi^3, \xi(\xi-1)^2 l, 3\xi^2 - 2\xi^3, \xi(\xi^2 - \xi)l\right], \tag{37}$$

where

$$\xi = \frac{x}{l} \quad (0 \leqslant x \leqslant l). \tag{38}$$

The finite element matrices $\boldsymbol{M}$, $\boldsymbol{C}_{\mathrm{G}}$, $\boldsymbol{C}_{\mathrm{V}}$ and $\boldsymbol{K}$ are given by

$$\begin{aligned}
\boldsymbol{M} &= \frac{\rho A l}{420}\begin{bmatrix} 156 & 22l & 54 & -13l \\ & 4l^2 & 13l & -3l^2 \\ & & 156 & -22l \\ \text{sym} & & & 4l^2 \end{bmatrix}, \qquad \boldsymbol{C}_{\mathrm{G}} = \frac{\rho A c}{30}\begin{bmatrix} 0 & 6l & 30 & -6l \\ -6l & 0 & 6l & -l^2 \\ -30 & -6l & 0 & 6l \\ 6l & l^2 & -6l & 0 \end{bmatrix}, \\
\boldsymbol{C}_{\mathrm{V}} &= \frac{1}{l^3}\begin{bmatrix} 12\eta I & 6\eta I l & -12\eta I & 6\eta I l \\ & 4\eta I l^2 & -6\eta I l & 2\eta I l^2 \\ & & 12\eta I & -6\eta I l \\ \text{sym} & & & 4\eta I l^2 \end{bmatrix}, \qquad \boldsymbol{K} = \frac{EI}{30l^3}\begin{bmatrix} K_{11} & K_{12} & K_{13} & K_{14} \\ & K_{22} & K_{23} & K_{24} \\ & & K_{33} & K_{34} \\ \text{sym} & & & K_{44} \end{bmatrix},
\end{aligned} \tag{39}$$

where

$$\begin{aligned}
&K_{11} = -K_{13} = K_{33} = 360 + 36r - 36s, \\
&K_{12} = K_{14} = -K_{34} = 180l + 3rl - 3sl, \\
&K_{24} = 60l^2 - rl^2 + sl^2, \\
&K_{22} = K_{44} = 120l^2 + 4rl^2 - 4sl^2, \\
&r = \frac{Pl^2}{EI}, \qquad s = \frac{\rho A c^2 l^2}{EI}
\end{aligned} \tag{40}$$

Tables 1 and 2 compare the lowest five eigenvalues (i.e., $\lambda_1, \lambda_2, \ldots, \lambda_5$) of the one-span beam and the two-span beam, respectively, for two cases. The first case is when the viscoelasticity is not taken into account (i.e., $\eta = 0$) and the second case is when the viscoelasticity is taken into account (i.e., $\eta = 6.8 \times 10^{-4} E$, where $E = 2 \times 10^{11}\,\mathrm{N/m^2}$). Physically, $\eta = 0$ means that the beams are pure elastic, while $\eta \neq 0$ means that the beams are viscoelastic. For the SEM results, only one finite element is used for the one-span beam while two finite elements for the two-span beam. Tables 1 and 2 show that the present SEM results are identical to the exact analytical results (Karnovsky and Lebed, 2001). When the beams are pure elastic (i.e., $\eta = 0$),

Table 1
The lowest five eigenvalues of the simply-supported stationary one-span beam obtained by the present SEM, FEM and the exact theory (Karnovsky and Lebed, 2001)

η	Method	N	λ_1	λ_2	λ_3	λ_4	λ_5
0	Theory (exact)		3.444i	13.777i	30.998i	55.107i	86.105i
	SEM	1	3.444i	13.777i	30.998i	55.107i	86.105i
	FEM	10	3.444i	13.800i	31.014i	55.198i	86.445i
		20	3.444i	13.778i	30.999i	55.113i	86.127i
		50	3.444i	13.777i	30.998i	55.107i	86.106i
		100	3.444i	13.777i	30.998i	55.107i	86.105i
$6.8\times10^{-4}E$	SEM	1	$-0.025+3.444$i	$-0.405+13.771$i	$-2.052+30.930$i	$-6.486+54.724$i	$-15.836+84.636$i
	FEM	10	$-0.025+3.444$i	$-0.407+13.794$i	$-2.055+30.946$i	$-6.508+54.814$i	$-15.961+84.959$i
		20	$-0.025+3.444$i	$-0.405+13.772$i	$-2.052+30.931$i	$-6.488+54.730$i	$-15.844+84.658$i
		50	$-0.025+3.444$i	$-0.405+13.771$i	$-2.052+30.930$i	$-6.486+54.724$i	$-15.836+84.637$i
		100	$-0.025+3.444$i	$-0.405+13.771$i	$-2.052+30.930$i	$-6.486+54.724$i	$-15.836+84.636$i

Note: (1) N = number of finite elements, (2) $E=2\times10^{11}\,\mathrm{N/m^2}$.

Table 2
The lowest five eigenvalues of the simply-supported stationary two-span beam obtained by the present SEM, FEM and the exact theory (Karnovsky and Lebed, 2001)

η	Method	N	λ_1	λ_2	λ_3	λ_4	λ_5
0	Theory (exact)		3.444i	5.381i	13.777i	17.436i	30.998i
	SEM	2	3.444i	5.381i	13.777i	17.436i	30.998i
	FEM	10	3.446i	5.382i	13.800i	17.482i	31.244i
		20	3.444i	5.381i	13.778i	17.439i	31.014i
		50	3.444i	5.381i	13.777i	17.436i	30.998i
		100	3.444i	5.381i	13.777i	17.436i	30.998i
$6.8\times10^{-4}E$	SEM	2	$-0.025+3.444$i	$-0.062+5.380$i	$-0.405+13.771$i	$0.649+17.424$i	$-2.052+30.930$i
	FEM	10	$-0.025+3.445$i	$-0.062+5.382$i	$-0.407+13.794$i	$0.653+17.470$i	$-2.085+31.174$i
		20	$-0.025+3.444$i	$-0.062+5.380$i	$-0.405+13.772$i	$0.650+17.427$i	$-2.055+30.946$i
		50	$-0.025+3.444$i	$-0.062+5.380$i	$-0.405+13.771$i	$0.649+17.424$i	$-2.052+30.930$i
		100	$-0.025+3.444$i	$-0.062+5.380$i	$-0.405+13.771$i	$0.649+17.424$i	$-2.052+30.930$i

Note: (1) N = number of finite elements, (2) $E=2\times10^{11}\,\mathrm{N/m^2}$.

the FEM results indeed converge to the SEM results or to the exact analytical results as the total number of finite elements is increased up to about 100 for the one-span beam and about 50 for the two-span beam. This is also true for the viscoelastic beams with $\eta=6.8\times10^{-4}E$. This observation certainly confirms the extremely high accuracy of the present spectral element model.

4.2. Effect of viscoelasticity and moving speed on the stability

The eigenvalues for the one-span beam and two-span beam are illustrated in Tables 1 and 2, respectively. It is assumed that two beams are all stationary (i.e., $c=0\,\mathrm{m/s}$), but not subject to axial tension (i.e., $P=0\,\mathrm{kN/m}$). Tables 1 and 2 show that all eigenvalues are pure imaginary for pure elastic beams (i.e., when $\eta=0$). However, for the viscoelastic beams (i.e., when $\eta\neq0$), the all eigenvalues are complex with imaginary values of which magnitudes are slightly reduced due to the effect of viscoelasticity. This implies that the effect of viscoelasticity tends to make two stationary beams more stable with reduced natural frequencies.

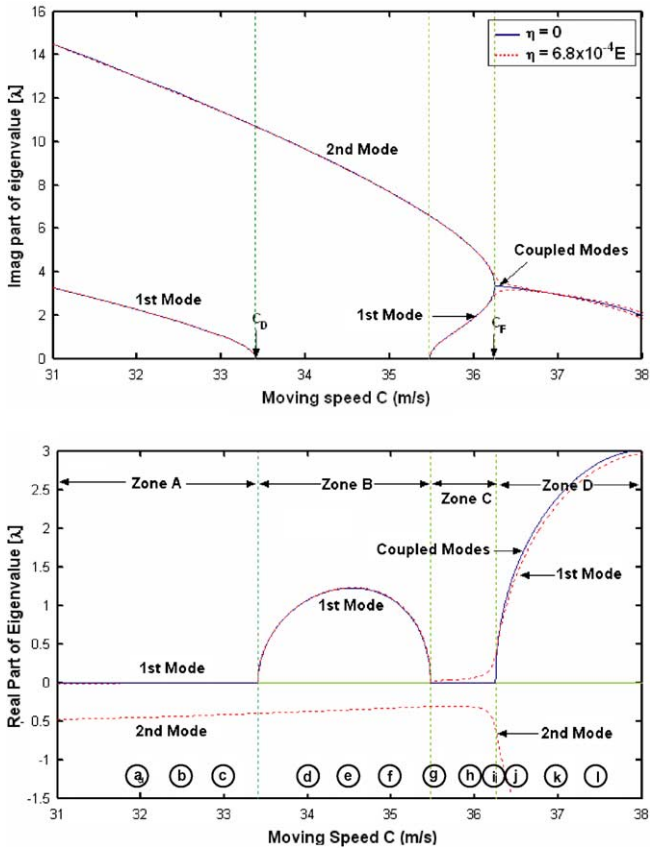

Fig. 4. Moving speed and viscoelasticity dependence of the lowest two eigenvalues of moving one-span beam subject to axial tension $P = 2.5\,\mathrm{kN/m}$: (—) for $\eta = 0$ and (···) for $\eta = 6.8 \times 10^{-4} E$ ($E = 2 \times 10^{11}\,\mathrm{N/m^2}$).

Fig. 4 shows the effects of the moving speed (c) and the viscoelasticity (η) on the variation of the lowest two eigenvalues (λ_1 and λ_2) of the moving one-span beam (Fig. 2a) subject to the axial tension $P = 2.5\,\mathrm{kN/m}$, while Table 3 on the stability of the corresponding two natural modes. Four zones (i.e., Zone A, Zone B, Zone C, and Zone D) are indicated in both Table 3 and Fig. 4, depending on the range of moving speed of beam. From Fig. 4 and Table 3, one may find the followings.

In Zone A, the imaginary parts of eigenvalues (i.e., natural frequencies) are reduced in magnitude as the moving speed is increased up to the lowest critical moving speed of about 33.40 m/s. This is true whether the beam is pure elastic or not. Thus, if the moving speed is kept below the lowest critical moving speed, the first natural mode and the second natural mode corresponding to λ_1 and λ_2 respectively, are always stable. It is interesting to observe that only the imaginary part of λ_1, i.e., the first natural frequency) vanishes completely as the moving speed reaches the lowest critical moving speed while its real part turns to positive from zero for the case of elastic beam (i.e., when $\eta = 0$) or to positive from negative for the case of viscoelastic beam (i.e., when $\eta \neq 0$). Physically this implies that the first natural mode becomes unstable by the divergence instability when the moving speed becomes equal or larger than the lowest critical moving speed of about 33.40 m/s. The lowest critical moving speed is called the divergence speed and denoted by c_{D}. The effect of viscoelasticity can be found numerically or analytically not to affect the divergence speed c_{D}. Because the divergence is the static instability, the divergence speed c_{D} for a simply-supported moving

Table 3
Effects of moving speed and viscoelasticity on the lowest two eigenvalues λ_1 and λ_2 of the moving one-span beam subject to axial tension $P = 2.5\,\mathrm{kN/m}$ ($E = 2\times10^{11}\,\mathrm{N/m^2}$)

Visco-elasticity η	Natural modes	Zones	Zone A				Zone B			Zone C				Zone D		
			$C < C_D = 33.40$				$C_D \leqslant C \leqslant 35.47$			$35.47 < C \leqslant C_F = 36.25$				$36.25 < C < 38.67$		
		Points (m/s)	a (32.0)	b (32.5)	c (33.0)	C_D (33.4)	d (34.0)	e (34.5)	f (35.0)	g (35.5)	h (36.0)	i (36.2)	C_F (36.25)	j (36.5)	k (37.0)	l (37.5)
0	First mode	$\mathrm{Re}[\lambda_1]$	0				+ve			0			+ve			
		$\mathrm{Im}[\lambda_1]$	+ve				0			+ve			+ve			
		Stability	Stable (neutral)				Divergence			Stable (neutral)			Flutter			
	Second mode	$\mathrm{Re}[\lambda_2]$	0				0			0			+ve			
		$\mathrm{Im}[\lambda_2]$	+ve				+ve			+ve			+ve			
		Stability	Stable (neutral)				Stable			Stable (neutral)			Flutter			
$6.8\times10^{-5}\,E$	First mode	$\mathrm{Re}[\lambda_1]$	−ve				+ve			+ve			+ve			
		$\mathrm{Im}[\lambda_1]$	+ve				0			+ve			+ve			
		Stability	Stable				Divergence			Flutter			Flutter			
	Second mode	$\mathrm{Re}[\lambda_2]$	−ve				−ve			−ve			−ve			
		$\mathrm{Im}[\lambda_2]$	+ve				+ve			+ve			+ve			
		Stability	Stable				Stable			Stable			Stable			
$6.8\times10^{-4}\,E$	First mode	$\mathrm{Re}[\lambda_1]$	−ve				+ve			+ve			+ve			
		$\mathrm{Im}[\lambda_1]$	+ve				0			+ve			+ve			
		Stability	Stable				Divergence			Flutter			Flutter			
	Second mode	$\mathrm{Re}[\lambda_2]$	−ve				−ve			−ve			−ve			
		$\mathrm{Im}[\lambda_2]$	+ve				+ve			+ve			+ve			
		Stability	Stable				Stable			Stable			Stable			

one-span beam can be readily derived from the static version of eigenvalue problem for the moving beam as follows (see Appendix A):

$$c_{\mathrm{D}} = \sqrt{\frac{EI}{\rho A}\left(\frac{\pi}{L}\right)^2 + \frac{P}{\rho A}}. \tag{41}$$

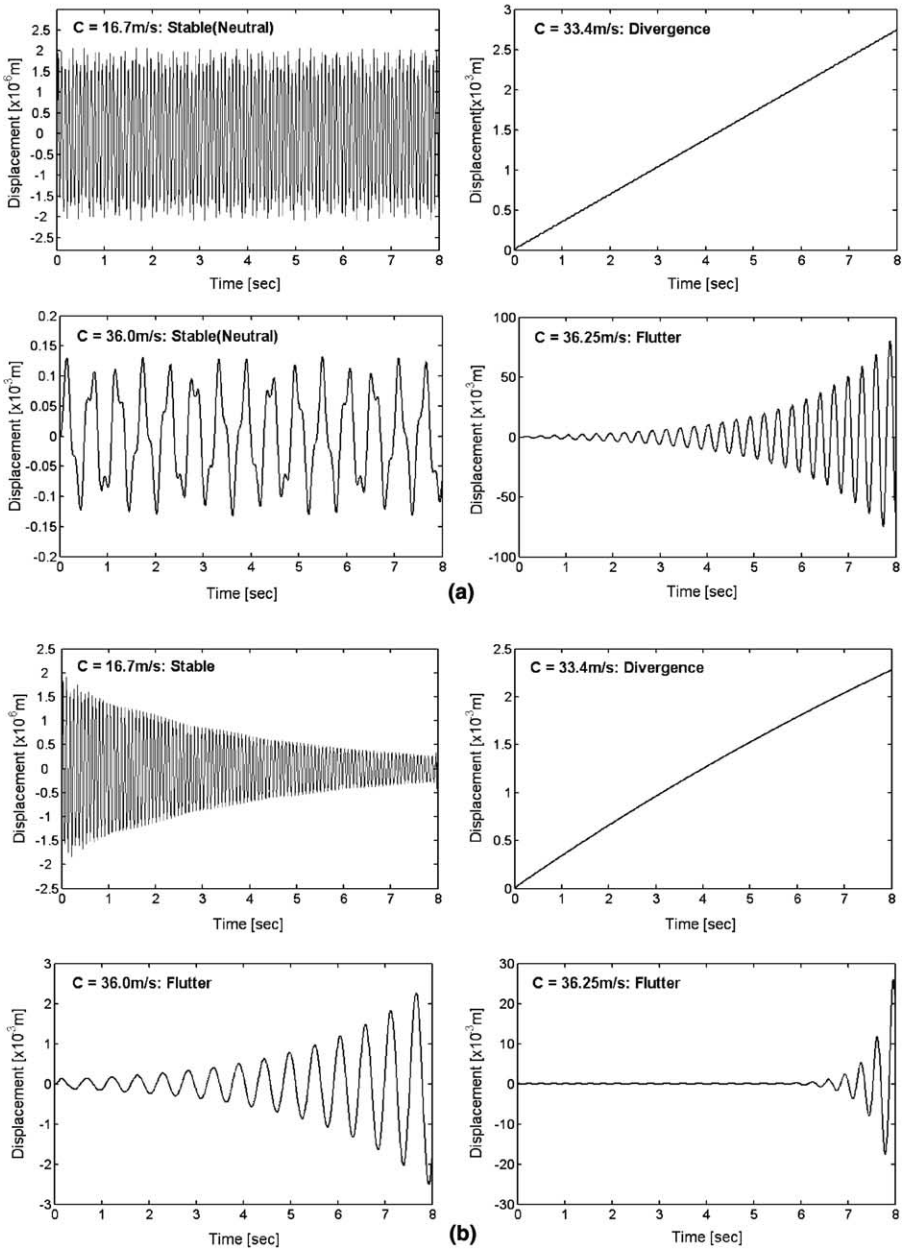

Fig. 5. Dynamic responses of the moving one-span beam subject to axial tension $P = 2.5\,\mathrm{kN/m}$ at various moving speeds. (a) Elastic beam ($\eta = 0$) and (b) viscoelastic beam ($\eta = 6.8 \times 10^{-4}E$).

The divergence speed computed directly from (41) is found to be identical to the numerically computed value 33.40 m/s, which is illustrated in Table 3 and Fig. 4.

In Zone B, the first natural mode is unstable with divergence instability, while the second natural mode keeps stable whether the beam is pure elastic (i.e., $\eta = 0$) or not (i.e., $\eta \neq 0$).

In Zone C, the imaginary parts of λ_1 and λ_2 are all positive. As the moving speed is increased, they merge gradually to each other. In other words, the first natural frequency increases while the second natural frequency decreases. In Zone C, the real part of λ_1 is zero for the case of elastic beam, but positive for the case of viscoelastic beam, while the real part of λ_2 is always negative in Zone C. This implies that, in Zone C, the second mode is always stable, and the first natural mode will be stable for the case of elastic beam and unstable (flutter instability) for the case of viscoelastic beam, which is the commonest case in practice. In other words, the viscoelasticity effect removes the second stable zone which may appear just after the divergence zone if elastic beam is elastic: this is probably the commonest case.

For the case of pure elastic beam ($\eta = 0$), two complex eigenvalues λ_1 and λ_2 completely merge to a single complex value at the boundary between Zone C and Zone D (i.e., at about $c = 36.25$ m/s). The imaginary part of the merged single complex eigenvalue is positive while the corresponding real part is zero. As the moving speed is increased beyond the critical moving speed of about 36.25 m/s, the imaginary part of the merged single complex eigenvalue decreases in magnitude while the real part increases. This observation implies that, for the case of elastic beam, the first and second natural modes are completely merged to a single coupled-mode which is unstable with flutter instability.

However, it is very interesting to investigate that the dynamics of the viscoelastic beam ($\eta \neq 0$) seems to be different in detail from that of the pure elastic beam ($\eta = 0$). In contrary to the case of pure elastic beam, two eigenvalues λ_1 and λ_2 of viscoelstic beam are not same and don't merge to a single value even though the moving speed is kept increasing beyond the critical moving speed of about 36.25 m/s. The imaginary

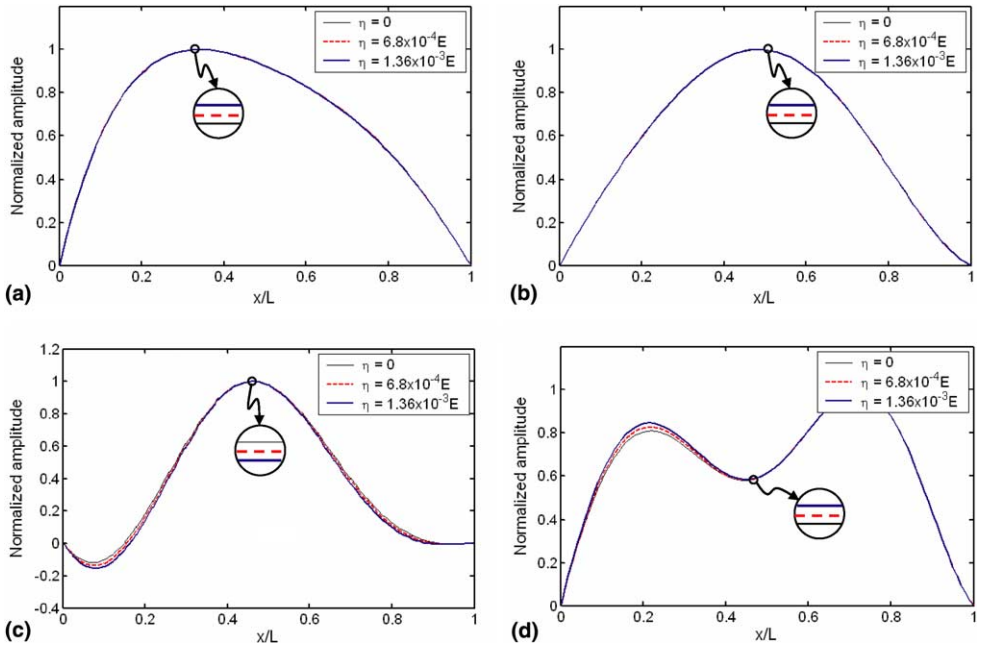

Fig. 6. Effect of viscoelasticity on the first natural mode shape of moving one-span beam subject to axial tension $P = 2.5$ kN/m. (a) $c = 32$ m/s (point a), (b) $c = 34$ m/s (point d), (c) $c = 36$ m/s (point h) and (d) $c = 36.5$ m/s (point j).

parts of λ_1 and λ_2 are all positive, but slightly different. The real part of λ_1 is positive while that of λ_2 is negative. This implies that the second natural mode keeps stable while the first natural mode of viscoelastic beam becomes unstable by the flutter instability as the moving speed is increased to become equal or grater than a critical moving speed of about 36.25 m/s, which is the flutter speed denoted by c_F. Thus, the coupled-mode flutter of a pure elastic beam should be distinguished from the first natural mode flutter of a viscoelastic beam.

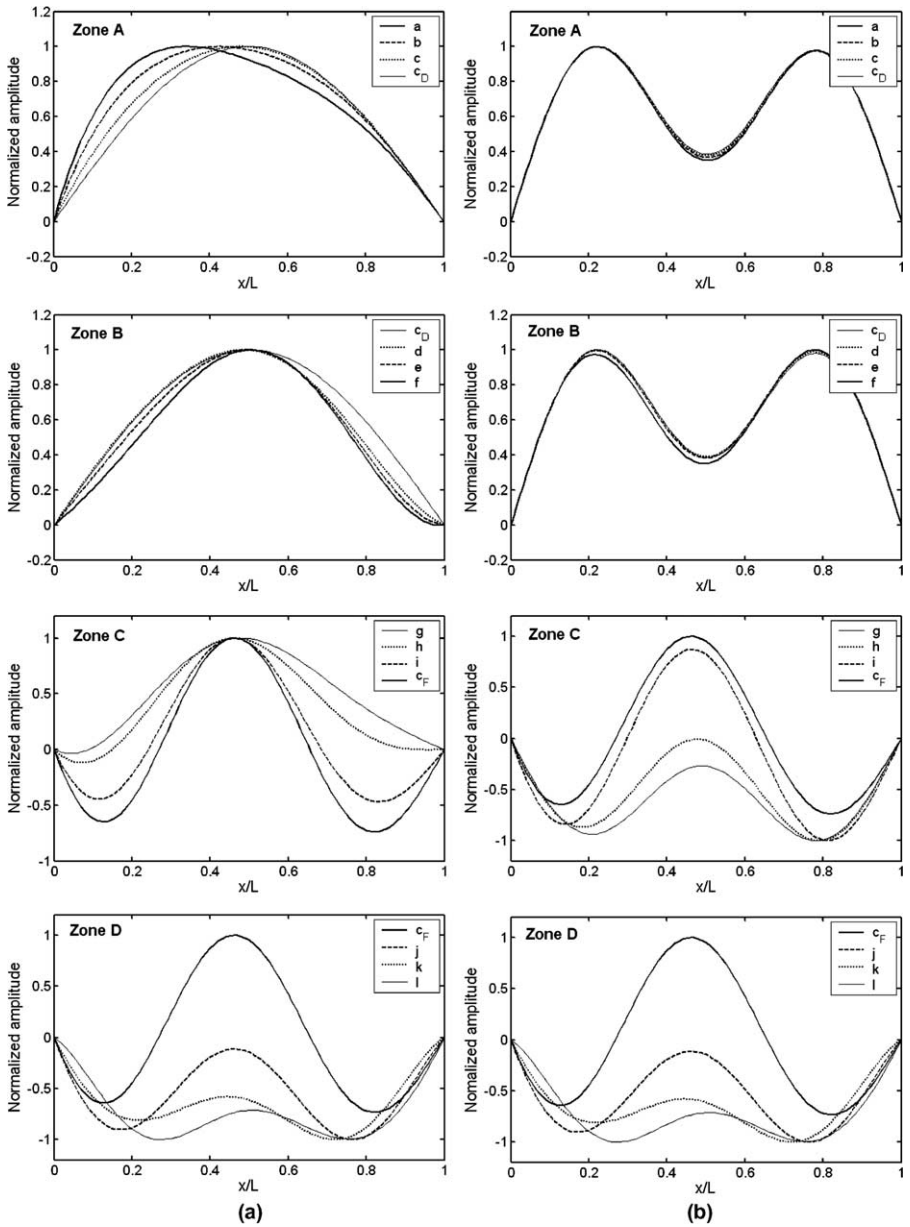

Fig. 7. Effect of moving speed on the first and second natural mode shapes of the moving elastic one-span beam ($\eta = 0$) subject to axial tension $P = 2.5$ kN/m. (a) First mode and (b) second mode.

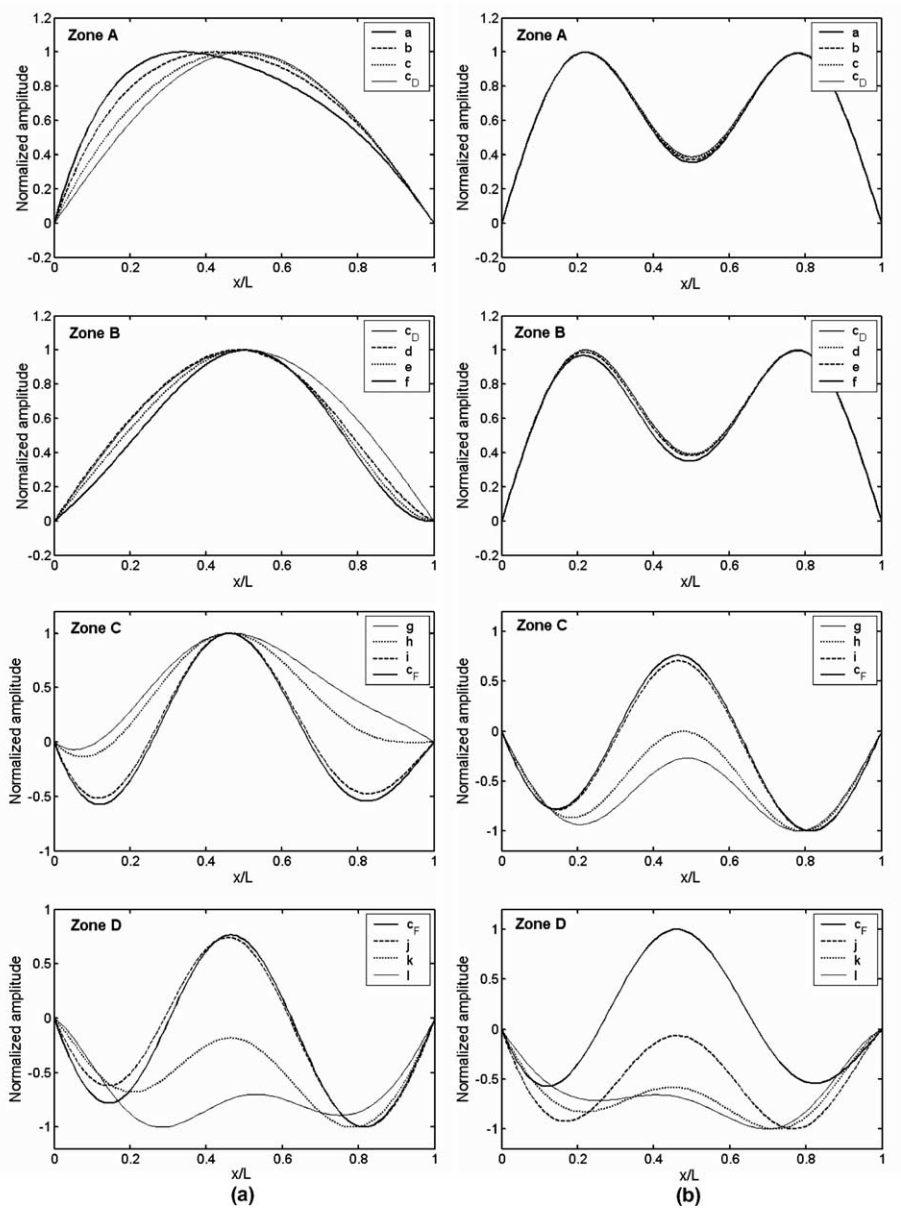

Fig. 8. Effect of moving speed on the first and second natural mode shapes of the moving viscoelastic one-span beam ($\eta = 6.8 \times 10^{-4} E$) subject to axial tension $P = 2.5\,\mathrm{kN/m}$. (a) First mode and (b) second mode.

Fig. 5(a) and (b) show the dynamic responses of the pure elastic one-span beam and the viscoelastic one-span beam, respectively, at various moving speeds: $c = 16.7\,\mathrm{m/s}$ in Zone A, $c = 33.4\,\mathrm{m/s}$ in Zone B, $c = 36.0\,\mathrm{m/s}$ in Zone C, and $c = 36.25\,\mathrm{m/s}$ in Zone D. As can be expected from Table 3 and Fig. 4, the dynamic response for the pure elastic beam is stable (strictly speaking, neutral) at $c = 16.7\,\mathrm{m/s}$, the divergence at $c = 33.4\,\mathrm{m/s}$, stable (neutral) at 36.0 m/s, and the flutter at $c = 36.25\,\mathrm{m/s}$. However, the dynamic response for the viscoelastic beam is somewhat different from that for the pure elastic beam. For instance, the viscoelstic beam is stable (not neural) at $c = 16.7\,\mathrm{m/s}$ and the flutter $c = 36.0\,\mathrm{m/s}$.

4.3. Effect of viscoelasticity on the natural modes

Fig. 6 compares the first natural mode shapes of the moving one-span beam at four moving speeds of the one-span beam subject to the axial tension $P = 2.5\,\mathrm{kN/m}$, depending on the degree of viscoelasticity η. The viscoelasticity tends to slightly distort the original natural mode shape of pure elastic beam (i.e., when $\eta = 0$). The changes of natural mode shapes due to the viscoelasticity are found to be relatively larger in flutter zones (i.e., Zone C and Zone D) when compared with the other zones of lower moving speeds. In general, however the effect of viscoelasticity on the change of natural modes seems to be not so significant.

4.4. Effect of moving speed on the natural modes

Fig. 7 compares the first and second natural mode shapes at various moving speeds for the elastic one-span beam subject to the axial tension $P = 2.5\,\mathrm{kN/m}$ (i.e., when $\eta = 0$), while Fig. 8 is for the viscoelastic one-span beam. The alphabets appeared in the legend of each figure denotes the different moving speeds of beam which are indicated in Table 3 as well as in Fig. 4. Form both figures; one may find that the natural modes gradually change their shapes as the moving speed of beam is increased. Comparing the first and second natural mode shapes at the same moving speed together as the moving speed of beam is increased, one may realize that two natural mode shapes are gradually changed to resemble to each other. In case of the elastic beam, Fig. 7 clearly shows that the first natural mode shape becomes exactly same as that of the second natural mode shape. Thus, as already discussed in the previous sub-section, the elastic beam will flutter in a completely merged single couple-mode when the moving speed is $c \geqslant c_{\mathrm{F}}$. However, in case of the viscoelastic beam, Fig. 8 shows the first two natural mode shapes resemble closely, but they are not exactly same. Thus, as also discussed in the previous sub-section, the viscoelastic beam will flutter only in the first mode when the moving speed is $c \geqslant c_{\mathrm{F}}$.

5. Conclusions

In this paper, the exact dynamic stiffness matrix so called spectral element matrix is derived to develop a spectral element model for the transverse vibration of an axially moving viscoelastic beam subject to an axial tension. The viscoelasticity of the beam material is represented in a general form by using the one-dimensional constitutive equation of hereditary integral type of viscoelastic material. The present spectral element model is then verified by comparing its solutions (e.g., eigenvalues) with those obtained by the conventional FEM as well as with those obtained by the exact theory. Numerical studies are conducted to investigate the viscoelasticity effect on the dynamics and stability of an example axially moving viscoelastic beam. The viscoelasticity effect is found to remove the second stable zone which may appear just after the divergence zone if elastic beam is elastic. It is also found that the first and second modes gradually change and merge to resemble to each other as the moving speed of beam is increased. As the result, only first natural mode becomes unstable with flutter in the case of viscoelastic moving beam, while a single coupled-mode flutter may occur for the case of pure elastic moving beam.

Appendix A

The divergence speed c_{D} at which the static instability occurs can be derived in a closed form by considering the existence of non-trivial equilibrium position, i.e., the corresponding static eigenvalue problem (Wickert and Mote, 1990; Oh et al., 2004).

The characteristic equation of the static eigenvalue problem for the simply-supported Kelvin–Voigt model moving beam can be reduced directly from (17), by putting $\omega = 0$ and also by using the relation $i\omega R(\omega)|_{\omega=0} = E$ from (34), as follows:

$$EIk^4 + (P - \rho Ac^2)k^2 = 0. \tag{A.1}$$

Four roots can be obtained from (A.1) as

$$k_1 = k_2 = 0, \qquad k_3 = -k_4 = \sqrt{\frac{\rho Ac^2 - P}{EI}} \equiv k. \tag{A.2}$$

The non-trivial equilibrium displacement can be then expressed in the form

$$W(x) = C_1 + C_2 x + C_3 e^{ikx} + C_4 e^{-ikx}. \tag{A.3}$$

The simply-supported boundary conditions are given by

$$\begin{aligned} &W(0) = 0, \qquad W''(0) = 0, \\ &W(L) = 0, \qquad W''(L) = 0. \end{aligned} \tag{A.4}$$

Applying (A.4) to (A.3) yields

$$\begin{bmatrix} 1 & 0 & 1 & 1 \\ 0 & 0 & -k^2 & -k^2 \\ 1 & L & e^{ikL} & e^{-ikL} \\ 0 & 0 & -k^2 e^{ikL} & -k^2 e^{-ikL} \end{bmatrix} \begin{Bmatrix} C_1 \\ C_2 \\ C_3 \\ C_4 \end{Bmatrix} = \begin{Bmatrix} 0 \\ 0 \\ 0 \\ 0 \end{Bmatrix}. \tag{A.5}$$

From the condition of the existence of nontrivial solutions of (A.5), the characteristic values can be obtained as

$$k_n = \frac{(2n-1)\pi}{L} \quad (n = 1, 2, 3, \ldots). \tag{A.6}$$

Substituting (A.6) into (A.1) gives the divergence speed c_{Dn} at which the divergence instability of the nth vibration mode occurs:

$$c_{\mathrm{Dn}} = \sqrt{\frac{EI}{\rho A}k_n^2 + \frac{P}{\rho A}}. \tag{A.7}$$

The lowest divergence speed c_{D} is given at $n = 1$ as follows:

$$c_{\mathrm{Dn}} = \sqrt{\frac{EI}{\rho A}\left(\frac{\pi}{L}\right)^2 + \frac{P}{\rho A}}. \tag{A.8}$$

References

Abolghasemi, M., Jalali, M.A., 2003. Attractors of a rotating viscoelastic beam. International Journal of Non-Linear Mechanics 38, 739–751.

Chen, T.M., 1995. The hybrid Laplace transform/finite element method applied to quasi-static and dynamic analysis of viscoelastic Timoshenko beams. International Journal for Numerical Method in Engineering 38, 509–522.

Christensen, R.M., 1982. Theory of Viscoelasticity. Academic Press, New York.

Dalenbring, M., 2003. Validation of estimated isotropic viscoelastic material properties and vibration response prediction. Journal of Sound and Vibration 265, 269–287.

Doyle, J.F., 1997. Wave Propagation in Structures: Spectral Analysis Using Fast Discrete Fourier Transforms. Springer-Verlag, New York.

Findley, W.N., Lai, L.S., Onarna, K., 1976. Creep and Relaxation of Nonlinear Viscoelastic Materials. North Holland, New York.

Flügge, W., 1975. Viscoelasticity, second ed. Springer-Verlag, Berlin.

Fung, R.F., Huang, J.S., Chen, Y.C., 1997. The transient amplitude of the viscoelastic traveling string: an integral constitutive law. Journal of Sound and Vibration 201 (1), 153–167.

Fung, R.F., Huang, J.S., Chen, Y.C., Yao, C.M., 1998. Nonlinear dynamic analysis of the viscoelastic string with a harmonically varying transport speed. Computers & Structures 66 (6), 777–784.

Haddad, Y.M., 1995. Viscoelasticity of Engineering Materials. Chapman & Hall, London.

Hou, Z., Zu, J.W., 2002. Non-linear free oscillations of moving viscoelastic belts. Mechanism and Machines Theory 37, 925–940.

Karnovsky, I.A., Lebed, O.I., 2001. Formulas for Structural Dynamics. McGraw-Hill, New York.

Lee, U., 2004. Spectral Element Method in Structural Dynamics. Inha University Press, Incheon, Korea.

Lee, U., Kim, J., Leung, A.Y.T., 2000. The spectral element method in structural dynamics. The Shock and Vibration Digest 32 (6), 451–465.

Le-Ngoc, L., McCallion, H., 1999. Dynamic stiffness of an axially moving string. Journal of Sound and Vibration 220 (4), 749–756.

Marynowski, K., Kapitaniak, T., 2002. Kelvin–Voigt versus Burgers internal damping in modeling of axially moving viscoelastic web. International Journal of Non-Linear Mechanics 37, 1147–1161.

Oh, H., Lee, U., Park, D.H., 2004. Dynamics of an axially moving Bernoulli–Euler beam: spectral element modeling and analysis. KSME International Journal 18 (3), 395–406.

Petyt, M., 1990. Introduction to Finite Element Vibration Analysis. Cambridge University Press, New York.

White, L., 1986. Finite element in linear viscoelasticity. In: Proceedings of the Second Conference on Matrix Method in Structural Mechanics, AFFDL TR 68150, pp. 489–516.

Wickert, J.A., Mote, C.D., 1988. Current research on the vibration and stability of axially moving materials. Shock and Vibration Digest 20, 3–13.

Wickert, J.A., Mote, C.D., 1990. Classical vibration analysis of axially moving continua. Journal of Applied Mechanics 57, 738–744.

Wittrick, W.H., Williams, F.W., 1971. A general algorithm for computing natural frequencies of elastic structures. Quarterly Journal of Mechanics and Applied Mathematics 24, 263–284.

Zhang, L., Zu, J.W., 1998. Non-linear vibrations of viscoelastic moving belts, Part I and II. Journal of Sound and Vibration 216 (1), 75–105.

Zhang, L., Zu, J.W., 1999. Non-linear vibrations of parametrically excited viscoelastic moving belts, Part I and II. Journal of Applied Mechanics 66 (2), 396–409.